Hydrodynamic Optimization of Ships with Retrofitted WASP-Systems

Hannes F. Renzsch
Friendship Systems AG, Germany, renzsch@friendship-systems.com

Fabian Thies
Friendship Systems AG, Germany

Abstract. Wind assisted ship propulsion has the potential to be one of the mainstays of emission reduction of commercial shipping. As it is not feasible to simply replace the fleet in service by newbuilds optimised for wind assisted propulsion, retrofitting WASP systems to existing ships holds great potential. In recent years several ships have been retrofitted in this way, but without taking into account the operation of the hull in yawed / heeled state due to the forces / moments generated by theses WASP systems. Consequently, the efficiency gain from retrofitting WASP systems to existing ships can be maximised by hull modifications of limited extent.
In this paper an efficient approach to evaluate potential hull modifications is presented. The approach is based on the prediction of hydrodynamic properties by response surfaces for the entire design range of modification by simulating a limited number of discrete variants. The impact of these modifications is evaluated in a bespoke simulation and optimisation platform taking into account the properties of the WASP system as well as the ships propulsion as well.

Keywords: RetroFit55; automatic optimisation; CAESES; WASP; hydrodynamics; CFD

NOMENCLATURE

c_D	Drag coefficient (ship coordinate system) [-]
c_R	Residual resistance coefficient (ship coordinate system) [-]
c_S	Sideforce coefficient (ship coordinate system) [-]
c_M	Moment coefficient [-]
k	Turbulent kinetic energy [m^2s^{-2}]

BREP	Boundary Representation
CII	Carbon Intensity Indicator
CFD	Computational Fluid Dynamics
EEXI	Energy Efficiency Index for Existing Ships
TWA	True Wind Angle [deg]
TWS	True Wind Speed [kts]
WASP	Wind Assisted Ship Propulsion

1. INTRODUCTION

Due to the ever increasing need to reduce harmful emissions from shipping, various approaches to use wind as a clean energy source for ship propulsion have come into the spotlight. Recently, several newbuilding projects or concepts integrating these systems have been presented or are close to delivery (Ayro, OceanBird/Orcelle, bound4blue, …).

While these newbuilds are great indicators of the progress made regarding wind (assisted) propulsion, they do not resolve the issue of the existing fleet in service. For these vessels already in service the options to reduce energy consumption and emissions by “classical” energy saving devices are quickly exhausted without yet fulfilling the required reductions due to upcoming restrictions (EEXI, CII). Still, for these vessels various options to retrofit WASP-systems are available as well (e.g., modular or palleted installations of Flettner rotors or wing sails).

But, when trying to reap the maximum benefit from these WASP-systems, the system itself is only one side of the coin. The hulls of these vessels are usually optimized to operate at zero leeway, zero heel, one or two speeds and one or two draughts. Due to this, they are not optimal to operate under the conditions and forces imposed by a WASP-system, by any means.

While initial retrofits of WASP systems do not appear to take these interactions into account a whole host of recently started EU-funded projects (e.g. RetroFit55, Whisper, …) aim to change this. Key to these projects is to evaluate the interaction of different approaches to save energy as well as their interaction with the existing ship. This paper focusses on a subset of these interactions, namely between WASP systems, hull and propulsion train and opportunities to optimise them.

This optimisation is based on the assumption that the hulls of merchant vessels in general are not optimised to operate at yaw and heel angles but to provide optimum performance in a straight line at a very limited range of speeds and draughts. This opens up the opportunity to gain improvements by very limited modifications, similar in concept to those applied in the quest for optimal slow steaming performance.

In the present study the hull shape is locally modified by the parametric modelling and optimisation software CAESES, the flow around the hull is simulated by a derivative of OpenFOAM and the interaction effects are evaluated using the performance prediction model ShipCLEAN.

2. MODELLING AND SIMULATION

A simulation platform was created consisting of parametric models, CFD software and a four degrees of freedom solver for performance prediction with and without WASP. The parametric models were set-up in CAESES which also stood for the process control, i.e., starting external processes and collecting results. The parametric model consists of a hull model based on the KVLCC2 with parametric form modification in both, the fore- and aftbody. OpenFoam was used as CFD software to compute the resistance in both, straight ahead and drifting conditions. The performance prediction including the 4 degree of freedom solution was obtained using parts of the ChaSE platform (formerly called ShipCLEAN, Tillig and Ringsberg (2020)), which were partially included in CAESES and partially run externally using python and octave. All created hull variants were simulated in OpenFoam at 0,3 and 6 degrees of drift to obtain the resistance and side force in those conditions. These results were used as a base to construct surrogate models to be utilized in optimization studies. ChaSE analysis were performed only for selected results and not included in the first step, since the aim is to perform optimization studies using different sail set-ups or appendages, requiring the bare hull side force and drag from the surrogate model, but a new solution from ChaSE.

2.1. PARTIALLY PARAMETRIC MODEL IN CAESES

The hull shape of the baseline vessel has been imported into CAESES as a step-model. Therefore, it is not a parametric model in itself. To modify the hull shape, various modelling functions of CAESES have been used.

2.1.1 Parametric Model of Deadwood

The deadwood is set up as a parametric model considering solely the extension beyond the skeg of the original hull shape (see Figure 1). If extending beyond the hull, it is automatically joined to the hull by a boolean operation. The extension is a free parameter to be varied by a design engine during the variation and optimisation process.

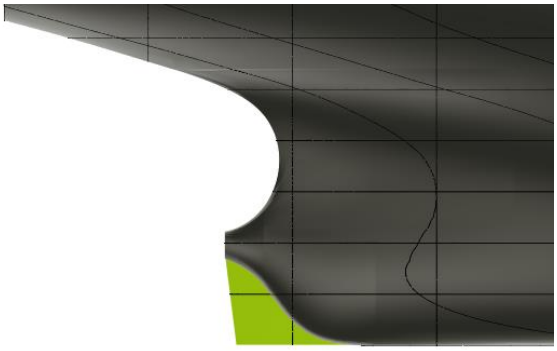

Figure 1. Example of deadwood extension.

2.1.2 Parametric Morphing of Stem Region

As the hull model itself is not described by a (partial) parametric model, so called BREP-Morphing has been applied to a defined part of the stem region. In this approach all surfaces within a box a modified proportionally to the deformation of this box (Figure 2) keeping the hull topology intact. The box itself is parametrised for modification by a design engine.

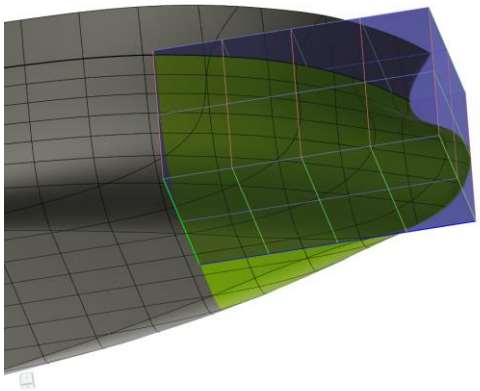

Figure 2. Stem region and deformation box for morphing, initial state.

Further to the definition by the box all transitions from morphed to fixed region below the waterline are defined to be C1-continuous, whereas C0 continuity is assumed to be sufficient above the waterline.

The deformation of the box – and the stem – is described by just three parameters varying the length of the bulb, the fullness of the waterlines forward and the rise of keel in the transition to the bulb. The possible range of modifications is shown in Chap. 3.1.

2.2. CFD Simulations Using OpenFOAM

To obtain the hydrodynamic forces and moments for each geometry variant the flow around was simulated using a highly modified version of OpenFOAM, Renzsch et al. (2017), Meyer et al (2016). To be able to use a validated simulation setup and accelerate turnaround times, the simulations were carried out in model scale. Following cases were computed:

- Baseline: Resistance curve, propulsion at two speeds, yaw sweep at one speed

- Variants: Yaw sweep at 15.5 kts, 0, 3, 6 degrees yaw

For the simulations, body-fitted split cartesian meshes of approx. 5.0mio cells, incl. boundary layer refinement, were generated using snappyHexMesh.

The free surface is captured by a volume of fluid approach with appropriate mesh refinement in the free surface region and bespoke differencing schemes to keep a sharp interface between air and water.

Model to full scale transformation has been computed by Reynold's correction for straight line resistance and assuming that side-force and added resistance coefficients are independent of scale.

Apart from selected cases run with propulsion by actuator disk to determine wake fraction and thrust deduction all simulations were carried out in resistance setup and without rudder as effects of rudder and propulsion are included analytically in ShipCLEAN.

2.3. Performance predictions

The performance, i.e., the required propeller propulsion power, of the hull variants with the WASP system fitted is evaluated using the generic simulation and modelling platform ChaSE (known as ShipCLEAN), which is described in more detail in Tillig and Ringsberg (2020). For all cases the total resistance of the ship including added resistances from waves, rudder and drift is obtained in the 4 degree of freedom solver based on the ChaSE platform. The solver also includes a sail trim optimizer ensuring the optimal sail trim of all individual sails with regards to obtain the lowest possible remaining thrust, i.e., the total resistance minus the sail thrust. The solver also evaluates the local flow speed and angle with respect to aerodynamic interaction effects. Detailed information about the underlying methods and the uncertainties can be found in Tillig and Ringsberg (2020) and Tillig and Ringsberg (2023).

3 BASELINE VESSEL AND VARIATIONS

As baseline vessel the well-known KVLCC2 (Van *et al.*, 1998) geometry (Figure 3) has been selected. This canonical hull geometry repeatedly used for CFD validation workshops is representative of 300k tdw tankers and bulk carriers as built in the 1990s. While not a particularly modern vessel, a significant number of similar ships is still in operation and potential candidates for retrofitting.

Figure 3. Canonical presentation of KVLCC2.

3.1. Hull Shape

Two modifications to the hull shape have been considered: The addition of a deadwood to the skeg and a modification of the forebody shape similar in principle to the “nose-jobs” regularly carried out on container vessels since the 2010s.

While the addition of a deadwood is a quite simple alteration, the modification of the stem shape, due to a tanker’s / bulk carrier’s particular layout (Figure 4), requires significant changes to the vessels structure and potentially forward tank / hold.

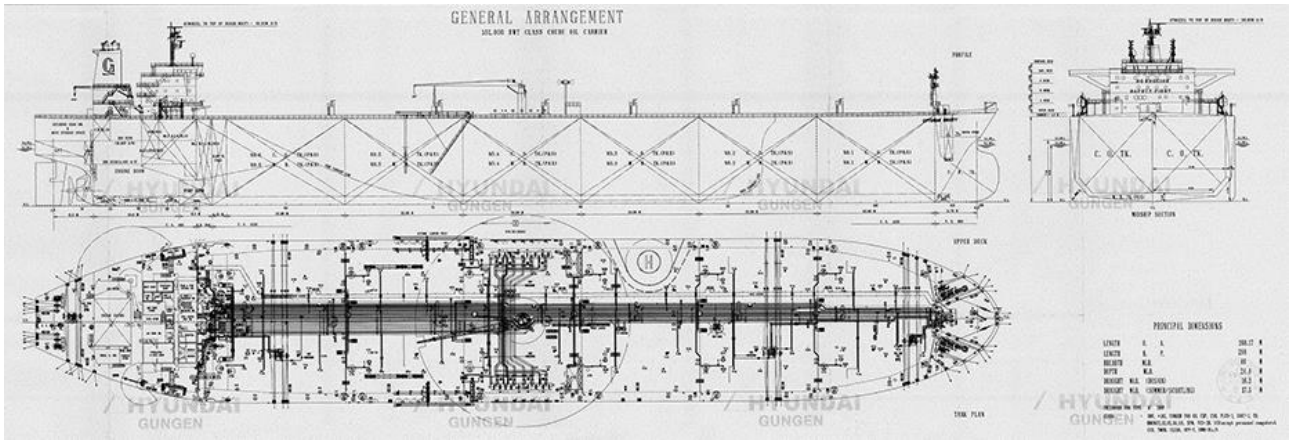

Figure 4. Typical layout of VLCC.

Selected areas of the hull shape are modified either by the addition of an extra part (deadwood) or morphing of a discrete region of the existing geometry (bow area). To properly capture the design space arising from the possible modifications with the least number of variants a Sobol sequence is used (Sobol, 1967). This is a quasi-random, space filling Design of Experiment (DoE) approach.

Examples depicting the range of modifications are shown in figures 5 to 8.

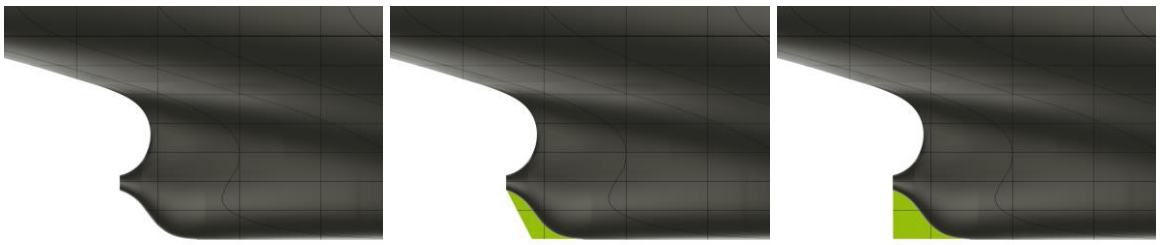

Figure 5. Range of deadwood extensions investigated.

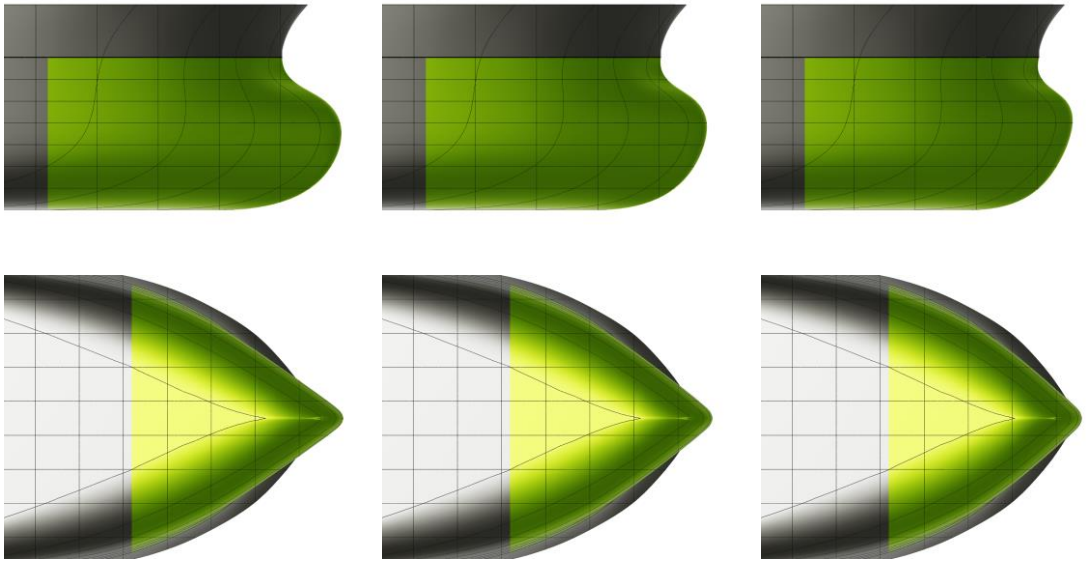

Figure 6. Variation of bulb length with length-scaling parameter.

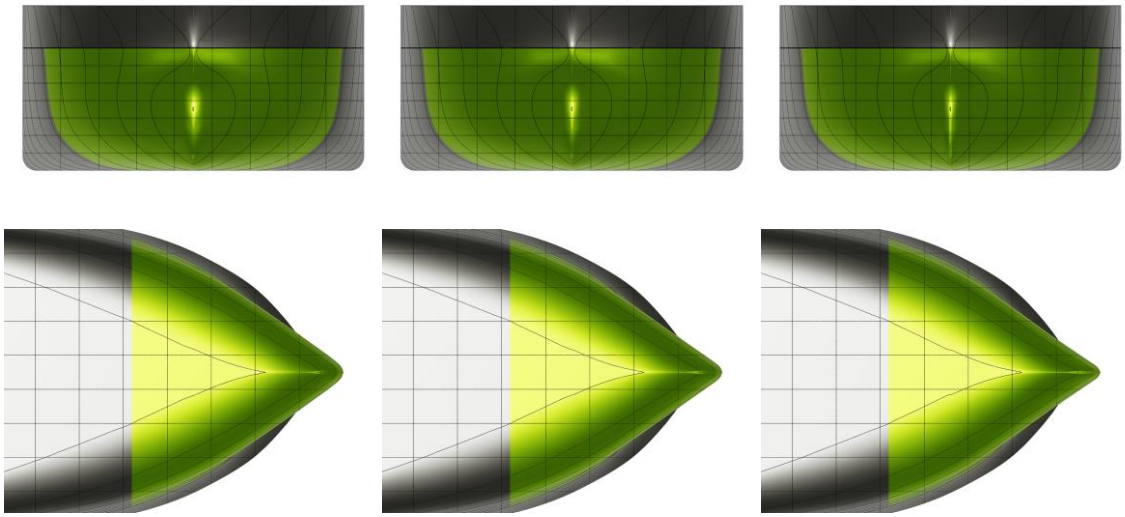

Figure 7. Variation of bulb fullness with beam-scaling parameter.

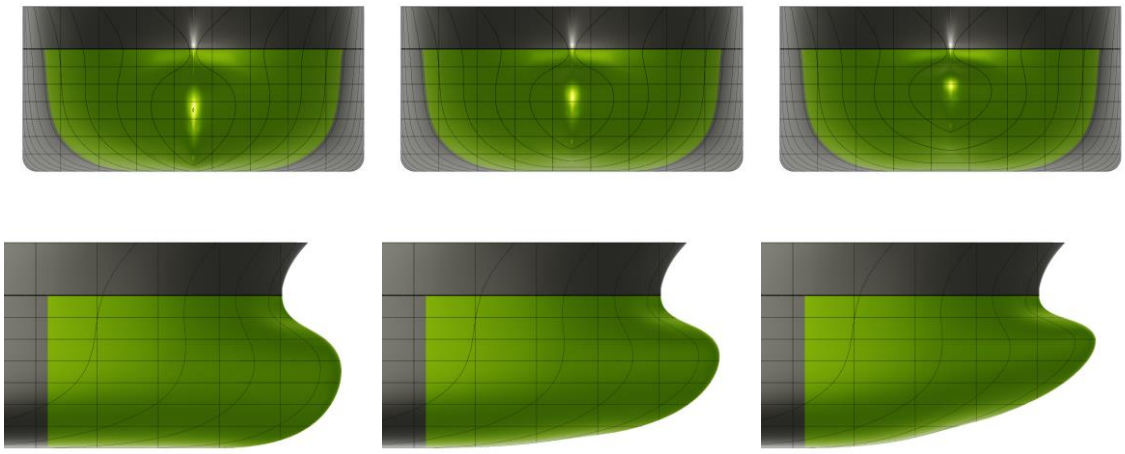

Figure 8. Variation of forward rocker with depth-scaling parameter.

3.2. WASP-System

Flettner rotors are used as a WASP-System in this study. The reason for this choice is that Fletter rotors are well validated in the ChaSE platform and there are already a number of ships sailing with Flettner rotors, it is thus regarded as a readily available and proven WASP technology. Six Flettner rotors with a diameter of 5 m and a height of 30m are installed on the ship, as illustrated in Figure 9.

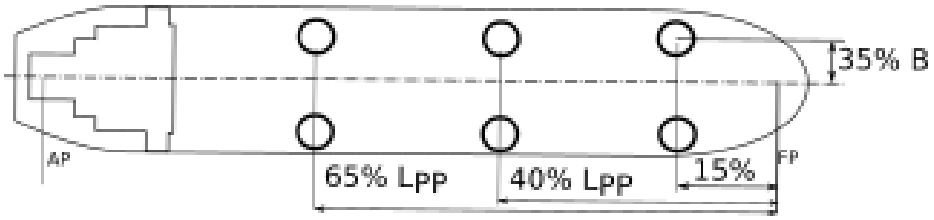

Figure 9. Layout of the Flettner rotors on the ship.

The lift and drag coefficients over the spin ratio of the rotors as used in the ChaSE platform are presented in Figure 10. The coefficients are based on results from CFD, model tests and full scale tests and proven to match very well in recent sea trial tests (WASP, 2023).

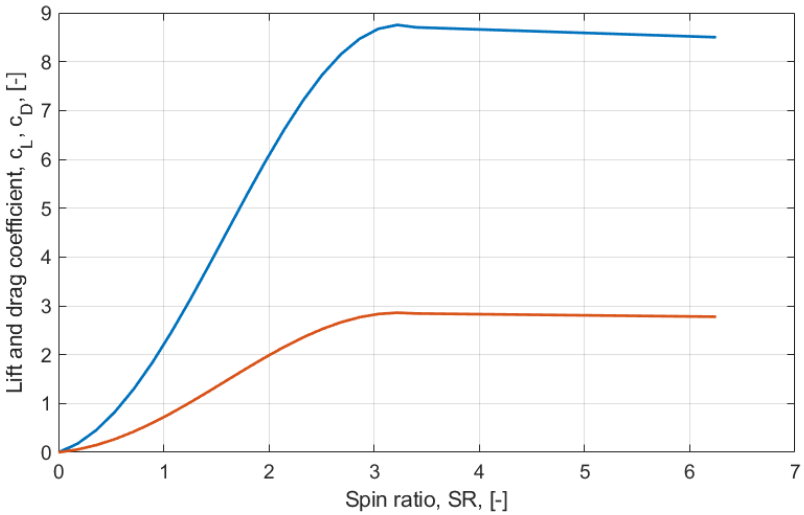

Figure 10. Lift and drag coeficients of the Flettner rotors.

4. SIMULATION RESULTS

In the following the simulation results for selected geometry variants are shown. To allow comparability the forces and moments have been normalised by dynamic pressure and the product of length and draught. To visualise the effect of the geometry variations on vortex formation in yawed conditions, plots of the total kinetic energy (*k*) have been chosen.

4.1. CFD-Simulations

The results of the CFD simulations depict discrete geometrical states as generated by the DoE (Sobol, see section 3.1) to efficiently capture the design space. While a pure design space exploration usually does not return an optimal design by itself, a multi-dimensional map of the results vs. the input variables can be generated. This map can subsequently be used for global optimisation without running further simulations. For a local optimisation, further simulations are generally required for local refinement of this map. It must be noted that all resistance and side force coefficients in this section are normalized using the planform area of the baseline vessel, i.e., its length times draft, instead of the wetted surface area.

4.1.1 Baseline Vessel

In the following figures and table the quantitative results of the CFD simulations carried out on the original KVLCC2 hull are shown. This study focusses on the side force and added resistance of a drifting ship. Thus, only resistance computations are performed. The effect of any changes in the propulsive performance due to the drift are neglected in this study.

Several aspects of the results are interesting:

- The resistance curve (Figure 11, extrapolated to full scale) has a pronounced bump slightly below the design speed.
- The wake fraction (Table 1) is quite high. This can be explained by the smalls scale of the model and correspondingly too thick boundary layer.
- While the behaviour of the yawing moment coefficient c_M is nicely linear over yaw, the side force coefficient c_S has a slight quadratic contribution, whereas the drag coefficient c_D behaves opposite to the expected (expected to be proportional to c_S^2). Instead, it is lower for 3 degrees of drift than for 6 and 0 degrees of drift, see Figure 12.

This gives rise to the question if the side force (and subsequently drag) behaviour is dominated by the formation of asymmetric bilge vortex patterns instead of behaving like a wing.

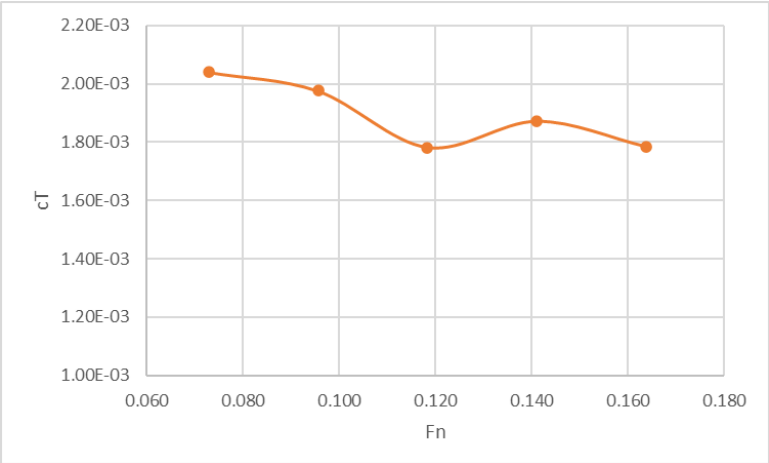

Figure 11. Resistance curve, bare hull, extrapolated to full scale.

Fn	w_M	t
[-]	[-]	[-]
0.096	0.3573	0.1854
0.141	0.4291	0.2280

Table 1. Taylor wake fraction (model scale) and thrust deduction.

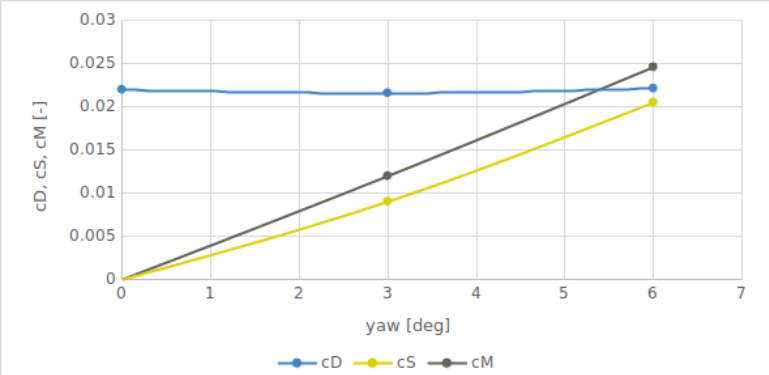

Figure 12. Lift, drag and moment coefficients (model scale) as function of drift.

4.1.2 Effect of Forebody Shape Variations

To compare the performance of the different variants, first the residual resistance at different drift angles, the added drag from drift and the created side force when drifting is compared. Afterwards, three promising variants are ranked against the baseline based on the net sail thrust in different wind conditions evaluated using the ChaSE platform.

Figure 13 presents the residual resistance, i.e., the total resistance with the frictional part deducted, of all variants at 0, 3 and 6 degrees of drift, relative to the corresponding values of the baseline hull. It is shown that the baseline hull has one of the highest resistances of all variants, when evaluated with 0 degrees of drift. At this condition, design 0014 features a residual resistance which is a whole 15% less than the value of the baseline hull. However, at 3 and 6 degrees of drift, the baseline hull is one of the best. This indicates that the forebody has a huge impact on not only the resistance at 0 degrees of drift, but also on the additional drag from drifting. The difference of the total resistance in full scale is up to 9.8% at 0 degrees and 6% at 6 degrees of drift.

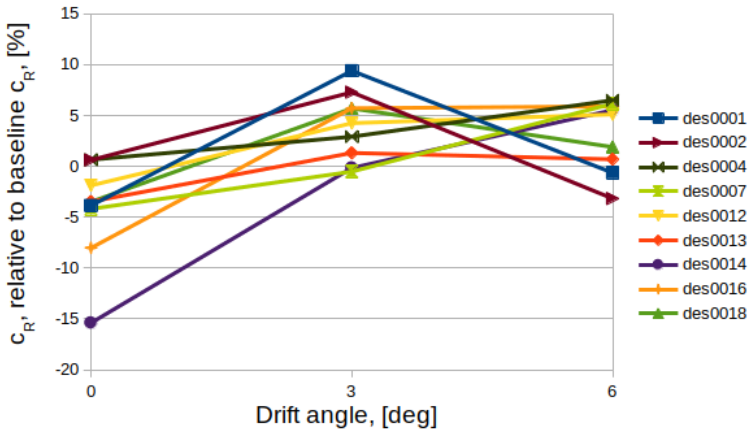

Figure 13. Residual resistance at 0, 3 and 6 deg of drift, relative to the baseline values

A closer look at the added resistance due to drift is provided in Figure 14, where the values evaluated by the ChaSE platform are included. The ChaSE platform evaluates the side force and drag based on an approach combining low aspect ratio wing theory and cross flow drag (Tillig and Ringsberg, 2020). It is shown that the behaviour of the hull's resistance differs largely. Some hulls, e.g., the baseline hull, have a lower resistance at 3 degrees of drift than at 0 degrees and a comparable resistance at 6 degrees. Other hulls have large added resistances at 3 degrees of drift, but only a slight increase of resistance at 6 degrees of drift (e.g. des0001). Two hulls show almost linear behaviour with increasing added resistance over the drift angle, des0014 and des0016. It is also shown that the values evaluated by ChaSE are rather high, but within the group of hulls up to 3 degrees of drift. However, at 6 degrees of drift the added resistance is overpredicted by ChaSE for all hull variants.

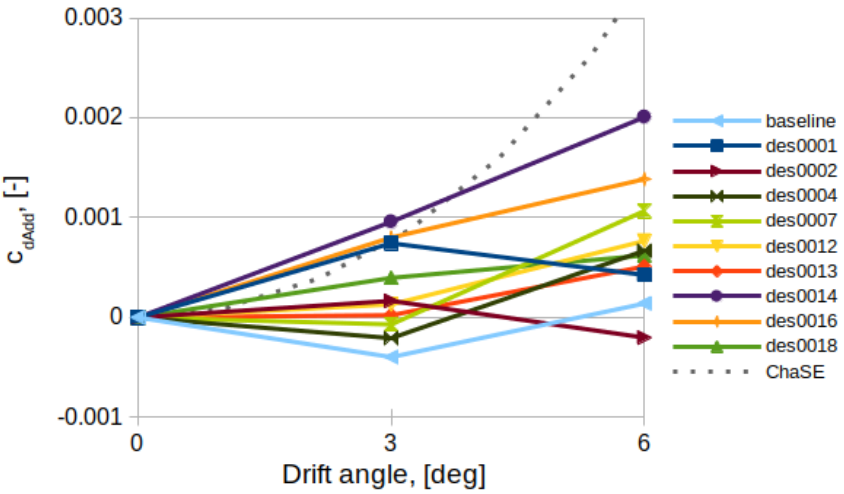

Figure 14. Added resistance due to drift

Compared to the resistance, the generated side force differs only slightly in between the variants, as shown in Figure 15. A maximal difference of less than 4% is observed at 6 degrees of drift. The value evaluated by ChaSE is slightly conservative.

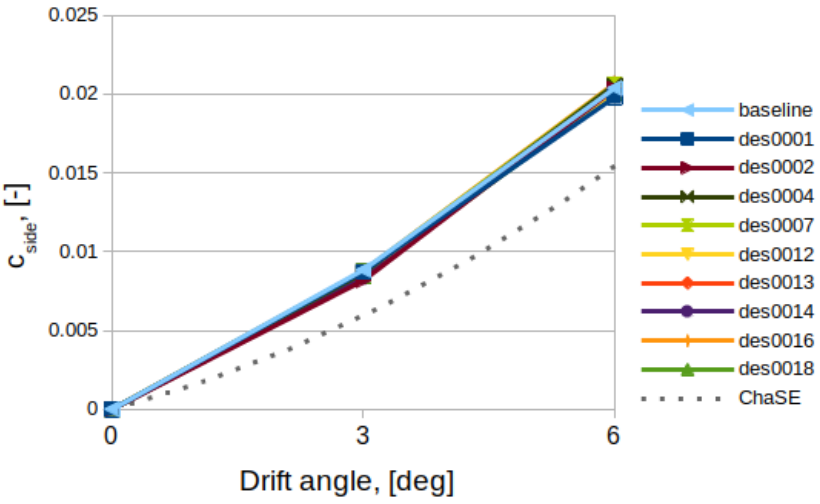

Figure 15. Side force generated by the drifting hulls

As suggested above, the side force seems to be mainly created from vortex formation along the bilge and centerline of the hulls. Thus, the small differences of the generated side force can also be observed with small differences in the turbulent kinetic energy (TKE), as shown in Figure 16.

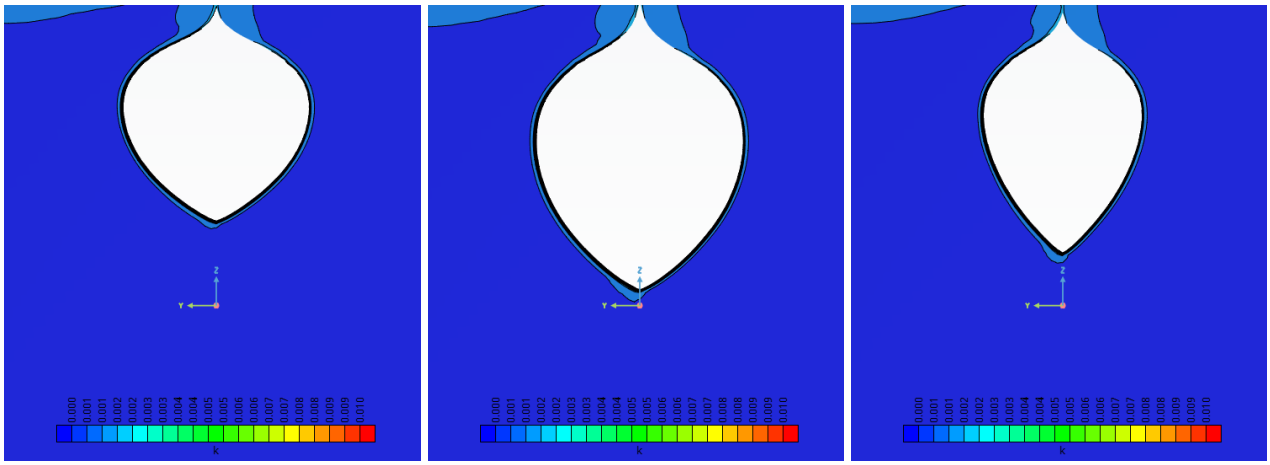

Figure 16. TKE at forward perpendicular at 6° drift (left to right: smallest c_S – des0001, baseline, largest c_S – des0016).

To further investigate the different additional drag of the hull variants, 2 variants are selected to be compared to the baseline in more detail. The selected variants are des0007, i.e., a design no added drag at 3 degrees but rather high added drag at 6 degrees of drift, and des0014, i.e., the design featuring an almost linearly increasing added drag.

As a first step, Figure 17 compares the wave patterns of the three variants at the different drift angles. Des0007 appears to have a favourable interference on the “suction” side which can cause the phenom that the resistance does not increase between 0 and 3 degrees of drift. This interference seems to vanish at 6 degrees, thus explaining the increase of resistance between 3 and 6 degrees of drift. The wave pattern of des0014 does not change much between 0 and 3 degrees, but the free waves are considerably lower on the suction side at 6 degrees. However, a large wave trough is created at the bow when drifting with 6 degrees. Thus, the influence of the free surface on the added resistance seems to be smaller for this design. It can also be seen that des0014 has much less waves than baseline and the des0007 at 0 degrees of drift, explaining the lower resistance. The baseline features almost constant wave patterns for all drift angles, thus the drop in resistance at 3 degrees of drift cannot be explained from the free surface plots.

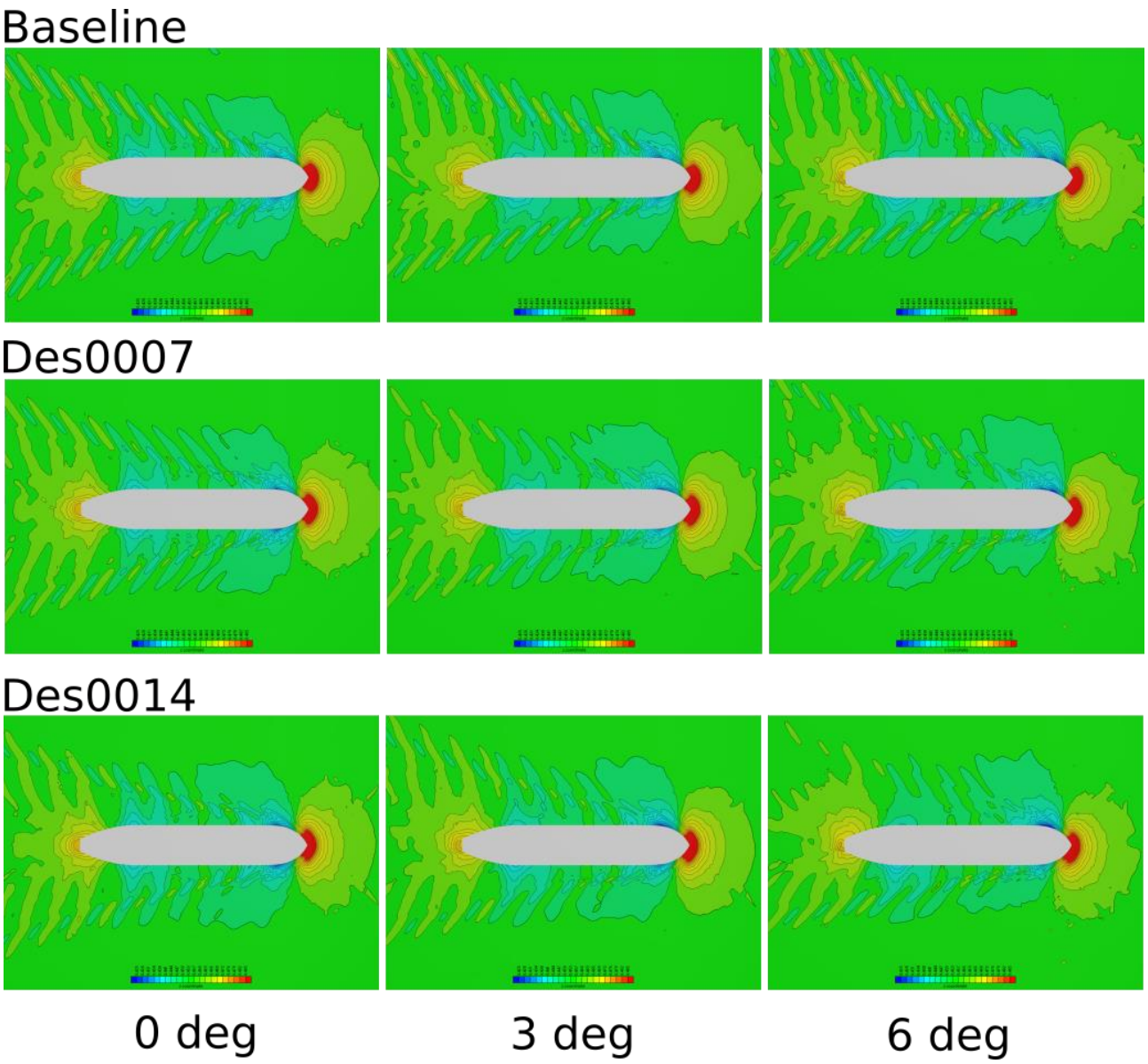

Figure 17. Wave patterns of the baseline, des0007 and des0014 at 0, 3 and 6 degrees of drift.

As a second step, the pressure distribution (dynamic pressure) at the forebody is compared in Figure 18. The baseline shows a much less pronounced low pressure field at the transition to the flat of bottom compared to the other variants. At 3 degrees of drift, the low pressure at the forward shoulder on the pressure side is reduced, which might help with decreasing the resistance. At 6 degrees of drift, a pronounced low pressure at the bottom is formed, which could result in some separation in this area, thus causing additional resistance. The trends are identical for the other hulls. However, the more pronounced low pressure fields on the bottom could give earlier separation, thus increasing the resistance, especially for des0014, which also features a large low pressure area at the forward shoulder of the suction side, as discussed earlier.

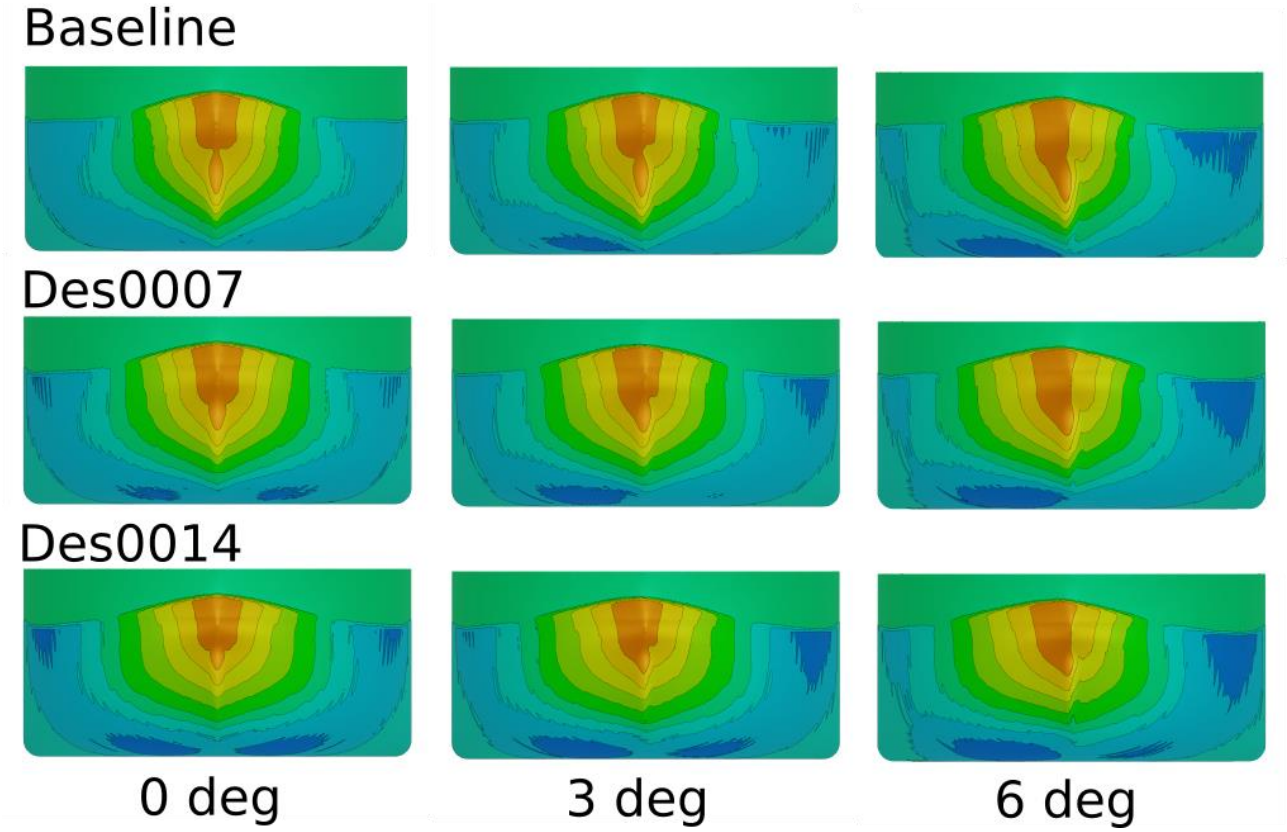

Figure 18. Pressure distribution (dynamic) at the bow of the baseline, des0007 and des0014 at 0, 3 and 6 degrees of drift.

As expected, the forebody variations did not affect the flow in the aftbody. The pressure distribution at the aftbody is presented for the baseline in Figure 19. The low pressure at the bilge completely disappears at drift. Thus, it must be assumed that the bilge vortex is only created at the suction side, which will considerably reduce the resistance at a drift angle.

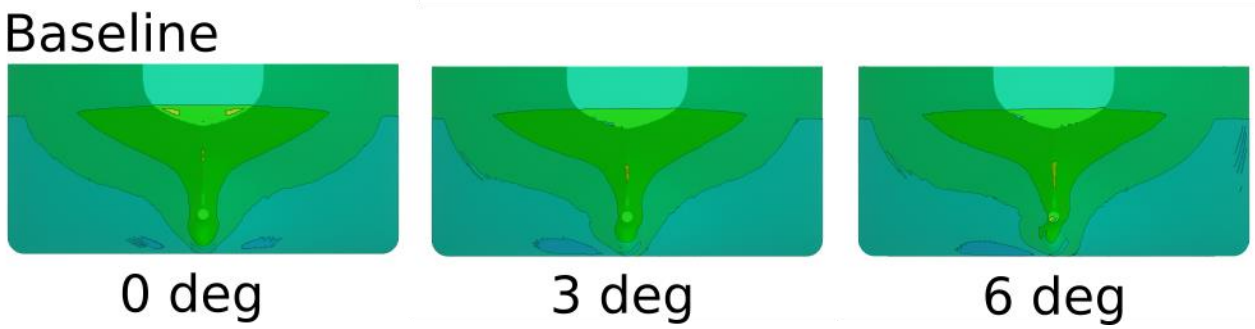

Figure 19. Pressure distribution (dynamic) at the of the stern of the baseline at 0, 3 and 6 degrees of drift.

In summary, the side force of a drifting hull seem to be mainly created by vortices formed around the bilge and the centerline of the hull. The forebody variations have only minor effects on the side force. The added drag is compromised out of different effects and thus difficult to predict. At a drift angle, the bilge vortex can vanish in the skeg region, which will decrease the resistance. A favourable (or unfavourable) interference might occur in the free surface wave pattern of a drifting ship and the low pressure fields at the transition from the bow to the flat of bottom become more pronounced when drifting. The values estimated by ChaSE correct in magnitude but pessimistic when compared to this ship. For drift angles larger than 3 degrees, the drag is overpredicted.

The effects of the presented differences on the performance of a WASP ship are evaluated using ChaSE. Three variants are selected for comparison: the baseline hull, which features a very low drag at 3 degrees of drift, des0014 which has the lowest drag at 0 degrees of drift and des0016 which has the highest side force at 6 degrees of drift. Both hull variants have considerably lower resistance at 0 degrees of drift, compared to the baseline but higher resistance at 6 degrees of drift. The required propulsion power from the propeller is compared in true wind angles (TWA) between 0-180 degrees and true wind speeds (TWS) of 5 and 20 kn. The resulst in terms of relative power (P_D over $P_{D\text{-baseline}}$) are presented in Figure 20.

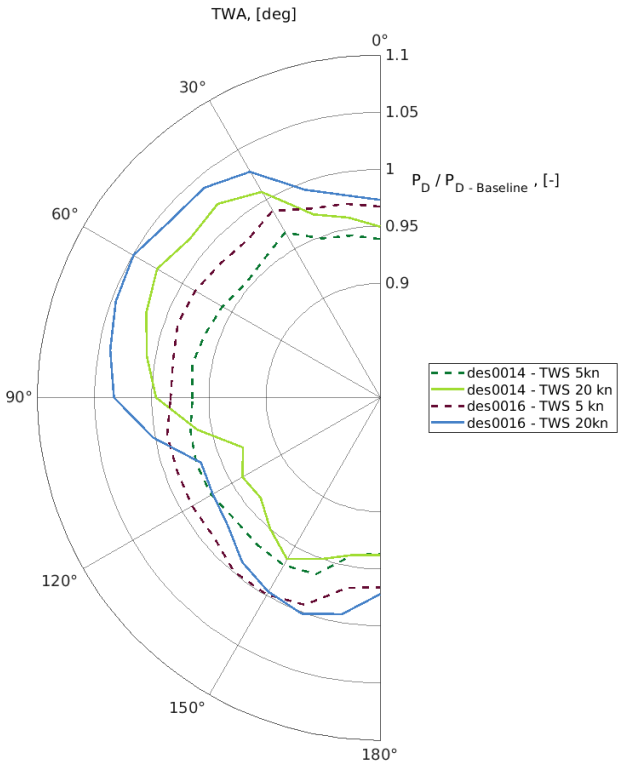

Figure 20. Polar plots of the required propulsion power from the propeller relative to the required power of the baseline hull.

The results show, that both hull variants require less power in low wind conditions, which is down to their lower resistance without a drift angle. However, in 20 kn of wind, the hull variants are better in any wind angles where the sails do not cause any large side forces, i.e., the ship does not drift. This is seen at TWA between 0-30 degrees and 110-180 degrees. In the TWA range of 30-90 degrees, both hull variants are up to 5 percent worse. This is due to the higher drag at a drift angle and because the sails create a large side force in these conditions. Obviously, the larger side force created by the hull des0014 does not affect the total performance as much as the higher drag.

4.1.2 Effect of a deadwood in the stern region

The effect of the deadwood in the stern region on the side force and added drag was estimated by creating two variants with different deadwood sizes. The side force and added drag relative to the side force and added drag of the baseline are presented in Figure 21. The results show that the deadwood considerably increases the created side force but also increases the additional drag. The increase of the drag and side force are most pronounced at 3 degrees of drift. One

explanation is, that the deadwood creates a strong vortex at lower drift angles, which is created at larger angles even without the deadwood.

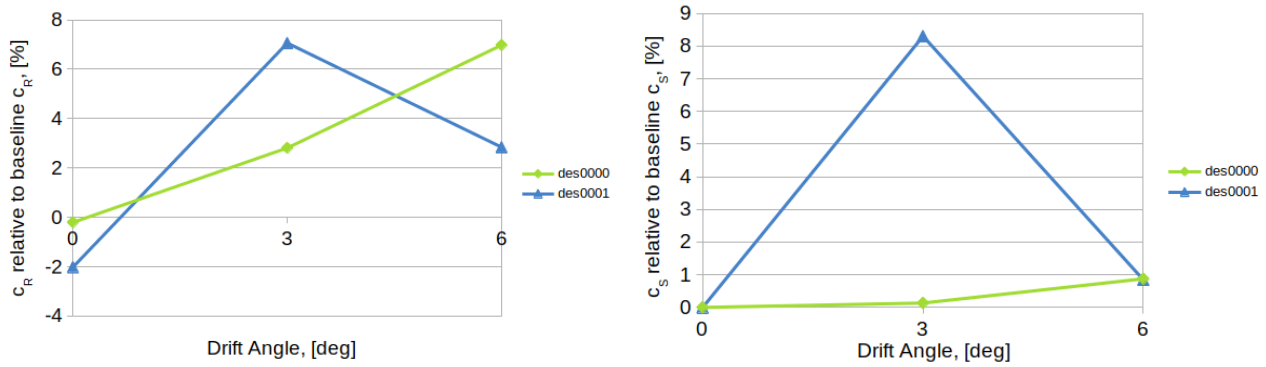

Figure 21. Residual resistance (left) and side force (right) of the variants with a deadwood relative to the baseline values.

To illustrate the effect of the deadwood, the turbulent kinetic energy (TKE) in the stern region is presented in Figure 22.

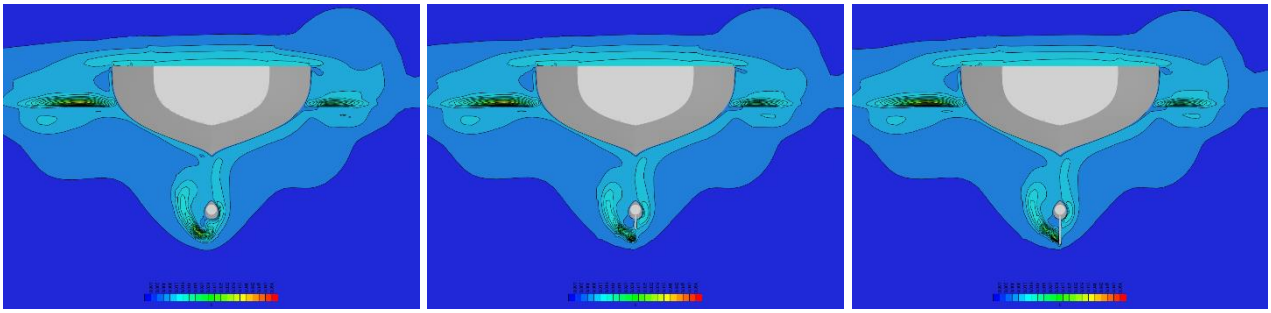

Figure 22. TKE at deadwood at 3° drift (left to right: baseline, increasing extension).

As for the forebody variations, the effect of the deadwood on the performance of a WASP ship is evaluated using ChaSE, in the same conditions as earlier. The resulst presented in Figure 23 show that the variants with a deadwood are worse in most conditions. As for the bow variations, this shows that it is more important to reduce the drag at drift than to increase the lift.

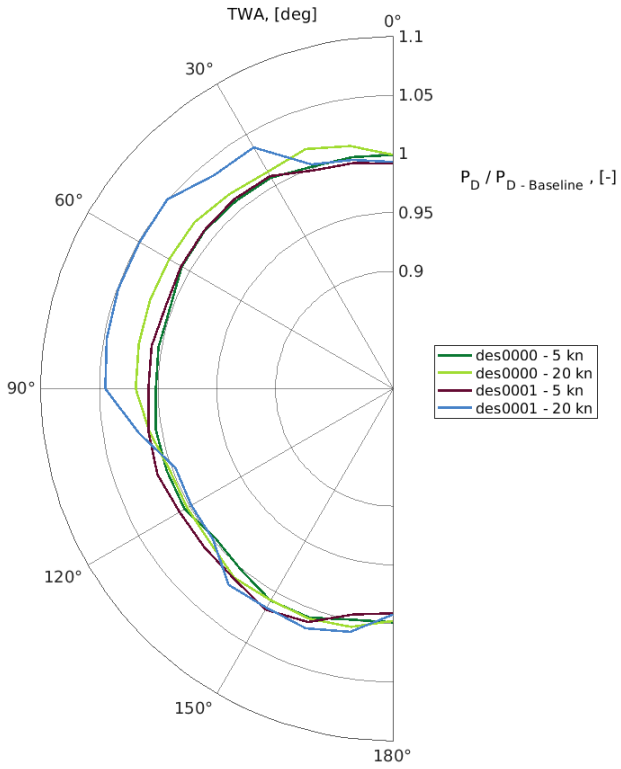

Figure 23. Polar plots of the required propulsion power from the propeller relative to the required power of the baseline hull.

5. CONCLUSIONS

The above simulation result show that shape modifications of limited regions of the bow area or just a deadwood attached to the stern can have a significant impact on the resistance and sideforce generated by a typical bulker / tanker hull. Further, it becomes apparent that the behaviour is significantly more complex than for hulls with high aspect wing-type appendages. The results from this study show that the added resistance caused by drifting is highly dependent on the forebody of the hull. Further, it was shown that the added resistance can be negative, i.e., that the hull has less resistance at a drift angle than without. It must be concluded that the drag of a drifting hull cannot accurately be captured with simple methods.

In this study, the rudder was excluded in the CFD computations, but included in the performance prediction using ChaSE/ ShipCLEAN. The rudder angle must be chosen to compensate the yaw moment introduced by the sails, thus adding the rudder would drastically increase the computational effort. However, a factor that should be researched in future work is the flow straightening by the hull, i.e., the difference between inflow angle to the hull and inflow angle to the rudder,

To increase the stability and increase comparability to model test results, all CFD calculations were performed in model scale. Since large parts of the side force is created by vortices, this might affect the results. Future work should compare the results for the side force and added resistance if evaluated in full and model scale. Further, only the resistance is evaluated. As shown in the result, the wake of the ship in the propeller plane is dramatically changed when the ship starts to drift. This will affect the propulsive performance. In the future, this effect should be researched. However, due

to the varying propeller load of a WASP ship, this requires a huge amount of CFD computations, which was outside of the scope of this study focussing on the side force.

Results from the performance prediction using ChaSE show a significant influence of the additional drag from drifting on the required propeller propulsion power. From the results it must be concluded that a low added resistance is by far more important than a high side force.

This study shows that the hydrodynamics of a WASP ship are complicated and that the resistance at a drift angle is of outmost importance. It must be concluded that a WASP ship must be optimized not only for low resistance at a straight line, but also for low resistance at drift.

6. ACKNOWLEDGEMENTS

As part of the HORIZON project “RetroFit55” this work received funds from the European Research Council (grant no. 101096068).

8. REFERENCES

Harries, S. and Uharek, S.. (2021). Application of Radial Basis Functions for Partially-Parametric Modeling and Principal Component Analysis for Faster Hydrodynamic Optimization of a Catamaran. *Journal of Marine Science and Engineering*, 9(10), 1069. https://doi.org/10.3390/jmse9101069

Meyer, J., Renzsch, H., Graf, K. and Slawig, T. (2016). Advanced CFD Simulations of free-surface flows around modern sailing yachts using a newly developed OpenFOAM solver. Proceedings of The 22nd Chesapeake Sailing Yacht Symposium, Annapolis, MD, USA

Renzsch, H., Meyer, J. and Graf, K.. (2017). Investigation of modern sailing yachts using a new free-surface RANS-code. Proceedings International Conference on Innovation in High Performance Sailing Yachts, 4th Edition, Lorient, FR

Sobol’,I.M. (1967). Distribution of points in a cube and approximate evaluation of integrals. U.S.S.R Comput. Maths. Math. Phys. 7: 86–112

Tillig, F., Ringsberg JW. (2020). Design, operation and analysis of wind-assisted cargo ships. Ocean Engineering, Volume 211, DOI: 10.1016/j.oceaneng.2020.107603

Thies, F.; Ringsberg, J.W. (2023). Retrofitting WASP to a RoPax Vessel—Design, Performance and Uncertainties. Energies 2023, 16, 673. https://doi.org/10.3390/en16020673

Van, S.H., Kim, W.J., Yim, D.H., Kim, G.T., Lee, C.J., and Eom, J.Y. (1998). Flow Measurement Around a 300K VLCC Model. Proceedings of the Annual Spring Meeting, SNAK, Ulsan, ROK

Van, S.H., Kim, W.J., Yim, G.T., Kim, D.H., and Lee, C.J. (1998). Experimental Investigation of the Flow Characteristics Around Practical Hull Forms. Proceedings 3rd Osaka Colloquium on Advanced CFD Applications to Ship Flow and Hull Form Design, Osaka, Japan

WASP (2023). WP3 Technical report, EU Interreg project “WASP”, to be published.